PCCP

ROYAL SOCIETY OF CHEMISTRY

PAPER

View Article Online
View Journal | View Issue

Cite this: *Phys. Chem. Chem. Phys.*, 2026, **28**, 7973

Characterization of F4TCNQ as a dopant in spiro-OMeTAD thin films by electron paramagnetic resonance spectroscopy

Shipra Prakash, *[a] Carl Hägglund, [b] Shaoqi Zhan,[a] Bhavya Rakheja, [b] Gerrit Boschloo [a] and Fikret Mamedov *[a]

Received 28th November 2025,
Accepted 5th March 2026

DOI: 10.1039/d5cp04633e

rsc.li/pccp

Spiro-OMeTAD is a widely used hole transport material in perovskite solar cells, contributing significantly to their high-power conversion efficiencies. In this study, Electron Paramagnetic Resonance (EPR) spectroscopy was employed to investigate F4TCNQ as a molecular dopant for Spiro-OMeTAD. The doping efficiency of F4TCNQ was examined by EPR spectroscopy by varying its concentration from 0.5 to 6 mol% in two different solvents: chloroform and chlorobenzene. Spiro-OMeTAD films prepared at these dopant concentrations in chloroform were additionally characterized with UV/VIS spectroscopic and ellipsometry measurements. EPR analysis of both solutions and films revealed that F4TCNQ doping is more effective in chloroform than in chlorobenzene, indicating a strong solvent influence on the doping efficiency of spiro-OMeTAD by F4TCNQ. Furthermore, an ambient air stability study was performed on F4TCNQ-doped spiro-OMeTAD films and compared with films containing conventional additives such as *t*BP, LiTFSI, and FK209. The results demonstrate that F4TCNQ serves as an efficient single dopant alternative to traditional additive mixtures. Results are discussed in the context of EPR spectroscopy as a powerful tool for identifying effective dopants for hole transport material thin films and elucidating the role of solvent–dopant interactions in determining doping efficiency.

Introduction

Organic–inorganic hybrid perovskite materials have gained much popularity for their light-harvesting and charge-carrier generation capabilities.[1,2] Photovoltaic solar cells (PSCs) based on organic–inorganic hybrid perovskites like methylammonium lead iodide ($MAPbI_3$, MAPI) have shown remarkable increase in efficiency during the last decade, with recently reaching a maximum above 26%.[3–6] Hole transport material (HTM) employed in methylammonium lead iodide ($MAPbI_3$, MAPI) and formamidinium lead iodide ($FAPbI_3$, FAPI) PSCs has contributed towards a significant increase in efficiency and stability of these devices.[7–10] In the n–i–p solar cell device architecture, one of the most common HTMs utilized for MAPI and FAPI devices is 2,2′,7,7-tetrakis (*N*,*N*-di-p-methoxyphenylamine)-9,9′-spirobifluorene (spiro-OMeTAD, Fig. 1a).[8,9] HTM layer performs a very important role in this architecture (Fig. 1b). It produces a significant energetic barrier against the movement of electrons towards the positive terminal and reduces free charge carrier recombination.[10] Spiro-OMeTAD is a very good HTM material as it not only fulfills these roles but also can be easily processed through spin coating in an organic solvent.[7]

The hole transport performed by spiro-OMeTAD is firstly based on the creation of holes that requires the oxidation of spiro-OMeTAD to spiro-OMeTAD$^{\bullet+}$ which is a complex reaction dependent on light and oxygen.[7,11] To increase the hole conductivity in spiro-OMeTAD, p-type dopants are employed,[7,10] and currently, the most common dopant used is lithium bis-(trifluoromethylsulfonyl)imide (LiTFSI) (Fig. 1c).[9,10] The main disadvantage of LiTFSI is that it is hydrophilic[7,8] and Li^+ can penetrate the perovskite layer, leading to its faster degradation.[12] Another additive, *tert*-butylpyridine (*t*BP) (Fig. 1c) is added together with LiTFSI to prevent phase separation of LiTFSI in the solvent used for spin coating.[7] It has been observed that *t*BP can also act as a dopant.[8,13] Frequently, in solar cell applications, spiro-OMeTAD is p-doped with LiTFSI together with *t*BP. LiTFSI cannot directly oxidize spiro-OMeTAD and therefore to regulate the amount of spiro-OMeTAD$^{\bullet+}$ formed, cobalt complexes like tris (2-(1*H*-pyrazol-1-yl)-4-*tert*-butylpyridine)cobalt(III)tri[hexafluorophosphate] (FK209) (Fig. 1c), which can oxidize spiro-OMeTAD are added together with LiTFSI and *t*BP[7] making it a complex sequential reaction.

[a] *Department of Chemistry – Ångström Laboratory, Box 523, Uppsala University, Uppsala 75120, Sweden. E-mail: shipra.prakash@kemi.uu.se, shipraprakash@gmail.com, fikret.mamedov@kemi.uu.se*
[b] *Department of Materials Science and Engineering, Box 35, Uppsala University, Uppsala 75103, Sweden*

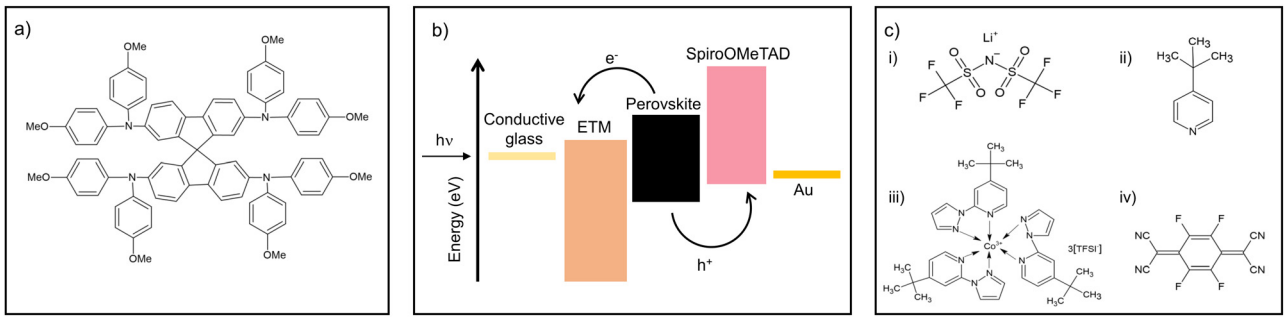

Fig. 1 Chemical structures of (a) spiro-OMeTAD (HTM), (b) schematic representation of n–i–p structure of perovskite cell with movement of hole towards the HTM, spiro-OMeTAD, and electron towards ETM after creation of charge carriers (holes and electrons) in the perovskite on absorption of light and (c) p-type dopants for spiro-OMeTAD that include (i) LiTFSI, (ii) *t*BP, (iii) FK209 and (iv) F4TCNQ.

At present, the search for new dopants that increase the device stability and achieve an equivalent PSC efficiency are of high importance. One of the p-type dopants that has been reported to give promising solar cell results is 2,3,5,6-tetrafluoro-7,7,8,8-tetracyanoquinodimethane (F4TCNQ) (Fig. 1c).[8,9] It has been used previously to dope spiro-OMeTAD in solid state dye-sensitized solar cells[14] and more recently in perovskite solar cells.[15,16] The addition of F4TCNQ provided more stable PSCs with a comparable efficiency to LiTFSI and *t*BP dopants. To evaluate the performance of different p-type dopants, it is necessary to understand molecular mechanism of the hole formation in each case. Also, since the molecular mechanism could be dissimilar in solution as compared to films, it is necessary to determine the mechanism and therefore the material properties of these dopants in films.

The oxidation of spiro-OMeTAD to spiro-OMeTAD$^{\bullet+}$ has been studied in solution and films by UV/VIS,[11,17–20] X-ray photoelectron,[21] FTIR and AFM spectroscopies.[22] The following mechanism has been proposed by Abate *et al.*[23] consisting of two steps. In the first step, spiro-OMeTAD$^{\bullet+}$ is formed by oxidation of spiro-OMeTAD to spiro-OMeTAD$^{\bullet+}$ as described in eqn (1). This is a reversible process and is influenced by light and thermal activation. In the presence of LiTFSI, the second step takes place where spiro-OMeTAD$^{\bullet+}$ TFSI$^{\bullet-}$ and Li_xO_y are formed.

$$\text{Spiro-OMeTAD} + O_2 \leftrightarrows \text{Spiro-OMeTAD}^{\bullet+}O_2^{\bullet-} \quad (1)$$

$$\text{Spiro-OMeTAD}^{\bullet+}O_2^{\bullet-} + \text{LiTFSI} \rightarrow \text{Spiro-OMeTAD}^{\bullet+}\text{TFSI}^{\bullet-} + Li_xO_y \quad (2)$$

Later studies based on spectroelectrochemistry and spectrophotometric measurements have observed the presence of two oxidized states (+1 and +2) in spiro-OMeTAD films.[11,19,24] Analysis of single crystals of spiro-OMeTAD^{+} and spiro-OMeTAD^{2+} combined with DFT calculations have given information on the delocalization of the hole on the spiro-OMeTAD molecule and hole transport process.[25,26] More recently, higher oxidation states (+3, +4) of spiro-OMeTAD in solution were identified and assigned by spectroelectrochemistry to different absorption bands.[27]

The mechanism of doping by F4TCNQ is different and does not require oxygen. F4TCNQ acts as an oxidant and therefore receives an electron from spiro-OMeTAD forming a charge transfer (CT) complex.[14–16] The CT complex later dissociates resulting in spiro-OMeTAD$^{\bullet+}$. UV/VIS spectroscopic measurements of spiro-OMeTAD doped with F4TCNQ in solution have assigned the peaks due to F4TCNQ negative polaron to the absorption maxima above 700 nm.[14–16] Considering that the HOMO level of spiro-OMeTAD and LUMO level of F4TCNQ are almost degenerate,[14–16] doping with F4TCNQ should initially produce a CT complex. However, it is not completely clear if the CT complex also contributes to the absorption bands at these wavelengths. In addition, F4TCNQ-doped spiro-OMeTAD has also been studied in solid state dye-sensitized and perovskite photovoltaic cells.[14–16] The studies suggest that F4TCNQ is more stable than LiTFSI as dopant and leads to an increase in conductivity of spiro-OMeTAD. Any solvent-dependent doping effects of F4TCNQ in spiro-OMeTAD films have not been reported yet.

One technique which is capable of directly detecting and quantifying radical formation, and therefore hole formation in spiro-OMeTAD is EPR spectroscopy. EPR spectroscopy is a direct, highly sensitive, and non-destructive magnetic resonance method to probe unpaired electron spins in organic radicals. EPR spectroscopy has been used previously to study spiro-OMeTAD$^{\bullet+}$ formation with LiTFSI doping and to estimate the doping efficiency of LiTFSI and FK209 on spiro-OMeTAD.[28,29] Moreover, EPR studies on *t*BP in spiro-OMeTAD showed that light excitation of *t*BP can cause de-doping of spiro-OMeTAD$^{\bullet+}$.[30]

In the present paper, EPR spectroscopy is performed on F4TCNQ doped spiro-OMeTAD films. In comparative experiments, other dopants such as *t*BP, LiTFSI, FK209 are also investigated. The results obtained with EPR spectroscopy are compared to measurements obtained by UV/VIS spectroscopy. In addition, influence of ambient air on spiro-OMeTAD films with different dopants is studied to determine the change in the amount of spiro-OMeTAD$^{\bullet+}$ with time. The results show that application of EPR spectroscopy is a useful and straightforward analytical method in characterizing HTM in solution and thin films for determining the doping efficiency and stability of p-type dopants in HTM thin films.

Materials and methods

Sample preparation

EPR spiro-OMeTAD solution preparation. 92 mg mL^{-1} spiro-OMeTAD solutions in chloroform (CF) or chlorobenzene (CB) were prepared to be doped with F4TCNQ. A stock solution of F4TCNQ (5 mg mL^{-1}, 18.10 mM) in acetonitrile was prepared one day previously and stored in the glove box. 400 μL of 92 mg mL^{-1} spiro-OMeTAD solution was doped with the stock solution of F4TCNQ to a final molar concentration of 0.5 mol%, 1.5 mol%, 3 mol% and 6 mol% of F4TCNQ. A control solution of only F4TCNQ (1 mg mL^{-1}, 3.62 mM) in acetonitrile was also prepared for EPR measurement. All the solutions were prepared in the glovebox under nitrogen atmosphere in dark glass vials on the day of the measurements. For the solution EPR measurements, 30 μL of the solution was taken in quartz tubes of inner diameter of 1.5 mm, with one end sealed with critoseal. These quartz tubes were inserted into X-band EPR quartz tubes (inner diameter 3 mm) and sealed inside the glovebox before the measurements. The samples were taken one by one directly after that for measurements.

EPR spiro-OMeTAD film preparation. Non-conductive, microscope glass slides were washed with three cycles of 30 min each of 1% Hellmanex, distilled water, acetone and ethanol sequentially and precut into 0.5 cm × 2.8 cm sections. After drying under nitrogen, they were UV ozone treated for 30 min before spin coating. 30 μL of spiro-OMeTAD doped with F4TCNQ as described above, was statically placed on the glass and spin coated at 4000 rpm for 20 s at acceleration of 2000 rpm s^{-1}. Additionally, a 70 mM spiro-OMeTAD solution in chlorobenzene with additives: *t*BP, 1.8 M LiTFSI in acetonitrile and 0.25 M FK209 in acetonitrile in the molar ratio of spiro-OMeTAD : *t*BP : LiTFSI : FK209 at 1 : 3.3 : 0.5 : 0.05 was prepared for spin coating. The spin coating was performed inside a nitrogen glove box. After spin coating, the spiro-OMeTAD thin film coated glass substrate was loaded in a 1 mL plastic pipette tip inside the glovebox, and both its ends were sealed. A 10 cm-long cylindrical wooden rod was affixed to one end of the tip to allow the sample to be suspended within the EPR cavity. The samples were stored overnight in the glovebox and measured the next day.

EPR spectroscopy

EPR measurements were performed at room temperature with EMX-micro spectrometer (Bruker BioSpin GmbH) equipped with an EMX-premium bridge and an ER4119HS resonant cavity. The solution measurements were performed at the following conditions: microwave frequency 9.86 GHz, microwave power 0.2 mW, modulation amplitude 1 G, 3 G and 5 G, 8 and 16 scans. Measurements on films were performed at the following conditions: microwave frequency 9.81 GHz, microwave power 0.2 mW, modulation amplitude 5 G, 12 scans. The contaminant signal from the glass substrate after UV ozone treatment (Fig. S1a) was measured under identical conditions to those used for the films and subtracted from each individual recorded spectrum before processing and simulation. An example of the subtraction is presented in Fig. S1b. The EPR spectra were simulated with an EasySpin package (version 6.0.1).[31]

UV/VIS spectroscopy

F4TCNQ-doped and undoped spiro-OMeTAD thin films deposited on glass substrates, as previously described in the EPR spiro-OMeTAD film preparation part, were used for UV/VIS spectroscopy measurements with the film side facing the light source.

Optical transmission and reflectance were measured with a Bentham PVE300 system using a monochromator and an integrating sphere. The investigated spectral interval was 300–1200 nm with a step size of 5 nm.

To determine the absorptance of the samples, the transmittance (T) and reflectance (R) of the films were measured across the wavelength range. Absorptance (A) was then calculated using the relation $A = (100 - T - R)\%$ for each film, and the resulting values were plotted as a function of wavelength.

Spectroscopic ellipsometry (SE) measurements and analysis

F4TCNQ-doped and undoped spiro-OMeTAD films on glass were used for SE measurements. The films were prepared as described in the EPR spiro-OMeTAD film section.

Standard SE measurements were performed using a Woollam RC2 tool, at 55, 60 and 65° angles of incidence in a 210–1690 nm spectral range. Scotch magic tape was applied to the back of the glass substrate to eliminate backside reflections. Data were collected for the glass only, and after deposition of spiro-OMeTAD films. Complementary measurements of the transmittance at normal incidence, using air as the reference, were also performed in the same setup after tape removal.

To enhance sensitivity to weak absorption, the SE data were combined with the transmittance data and the two data sets were fitted jointly in the CompleteEASE software, using a factor ×3 weight for the transmittance in the calculation of the root mean squared error (RMSE). This weighting was introduced to balance the ×6 times more data from SE (with the ellipsometric variables Ψ and Δ measured at 3 different angles), and was further motivated by the higher internal correlation of the latter data. Each layer of the model stack was fitted separately to the corresponding measurements, and then fixed in the further analysis. The glass substrate was modeled using a Cauchy layer with an Urbach tail to account for absorption below 300 nm wavelength. For the spiro-OMeTAD, thickness variations contributed to the higher errors in the fit.

The density functional theory (DFT) calculations

The DFT calculations were performed on spiro-OMeTAD molecule extracted from spiro-OMeTAD crystal structure[32] using the tuned long-range corrected ωB97X-D3BJ functional. Geometry optimization and spin density calculations were carried out with the 6-31G** basis set, while EPR calculations were performed at the wB97X-D3BJ/EPR-II level of theory using the RIJCOSX approximation for efficient evaluation of exchange integrals. All calculations were conducted using the ORCA

5.0 package.[33] The resulting spin density was visualized using the Avogadro program.

Results

EPR spectroscopy of spiro-OMeTAD after doping with F4TCNQ in solution

Spiro-OMeTAD solution prepared in two different solvents and containing different doping amounts of the dopant F4TCNQ was measured with EPR spectroscopy. The solubility of F4TCNQ in different solvents has been assessed previously using a range of solvents from acetonitrile, chloroform to toluene, and it was found that F4TCNQ showed a good solubility in acetonitrile.[34] In the present study, a series of solvents were also investigated and it was found that F4TCNQ was completely soluble in dichlorobenzene, acetonitrile and chloroform. However, it was not fully soluble in chlorobenzene. Thus, for F4TCNQ doping with spiro-OMeTAD, two solvent systems were chosen. Spiro-OMeTAD was prepared in chlorobenzene and chloroform, F4TCNQ stock solution in acetonitrile and added to spiro-OMeTAD solution to get a final doping of 1.5, 3 and 6 mol%.

The EPR spectra were obtained with a modulation amplitude of 1G and are presented in Fig. 2. EPR signals at a g value of 2.0025 (3519 G) from spiro-OMeTAD in chloroform (Fig. 2a) and chlorobenzene (Fig. 2b) can be assigned to spiro-OMeTAD$^{\bullet+}$. The assigned g value is similar to the one reported previously for spiro-OMeTAD$^{\bullet+}$ in films.[28] The spectra in Fig. 2a show a single derivative signal corresponding to spiro-OMeTAD$^{\bullet+}$ for all the concentrations. However, in Fig. 2b, the EPR spectra for doping concentrations of 1.5 mol% (blue) and 3.0 mol% (orange) of F4TCNQ, exhibit a clear hyperfine contribution from free F4TCNQ$^{\bullet-}$ radical. EPR spectrum of only F4TCNQ solution (1 mg mL^{-1}, 3.62 mM) in acetonitrile measured under similar conditions showed the presence of F4TCNQ$^{\bullet-}$ radical (Fig. S2). A g value of 2.0032 but no hyperfine structure is observed in this case possibly due to a high concentration of F4TCNQ. A g value of 2.0030 and hyperfine splitting of 4.4 and 3.1 MHz due to four equivalent fluorine and nitrogen atoms respectively for F4TCNQ$^{\bullet-}$ radical have been previously reported.[35] The EPR spectra in Fig. 2b were simulated (see also Fig. S3) using these parameters and a contribution of for the F4TCNQ$^{\bullet-}$ radical at 3, 7 and 12% was estimated in the spectra for 1.5, 3 and 6 mol% of F4TCNQ respectively. The spectra in Fig. 2b therefore show a mixture of F4TCNQ$^{\bullet-}$ anion and spiro-OMeTAD$^{\bullet+}$ cation radicals. It was observed that after a day, the contribution from free F4TCNQ$^{\bullet-}$ anion had completely disappeared. In the spectra from the spiro-OMeTAD in chloroform (Fig. 2a), no free F4TCNQ$^{\bullet-}$ anion radical has been observed. We have performed a series of experiments with different modulation amplitudes and microwave powers but did not observe hyperfine splittings due to the F4TCNQ$^{\bullet-}$ anion radical. Since, all the sample preparation procedures were kept constant, this indicates that the formation of spiro-OMeTAD$^{\bullet+}$ is different in the two solvents. Thus, chloroform is favoring the formation of spiro-OMeTAD$^{\bullet+}$, when F4TCNQ is used a dopant.

The amount of the spiro-OMeTAD$^{\bullet+}$ formed in the solution is proportional to the integrated area of the derivative signal. A plot of EPR signal obtained from the spectra for each doping concentration of F4TCNQ in two solvents, chloroform and chlorobenzene is presented in Fig. 2c. As mentioned above, the EPR spectrum in chlorobenzene contains contribution from F4TCNQ$^{\bullet-}$ radical. The contribution of F4TCNQ$^{\bullet-}$ radical at 3, 7 and 12% for 1.5, 3 and 6 mol% was subtracted prior to plotting the EPR signal area for chlorobenzene in Fig. 2c. In the case of chlorobenzene, the amount of spiro-OMeTAD$^{\bullet+}$ shows a linear increase with the increase in doping concentration of F4TCNQ (diamonds). Spiro-OMeTAD prepared in chloroform does not show a similar proportional increase for the radical formation with increase of F4TCNQ doping concentration (triangles). It can be also observed from the signal analysis that the amount of spiro-OMeTAD$^{\bullet+}$ formed in chloroform is significantly higher than in chlorobenzene. For a doping concentration of 1.5 mol% of F4TCNQ, it was 8 times higher (Fig. 2c). This result again strengthens our conclusion that the doping capacity of F4TCNQ is better in chloroform.

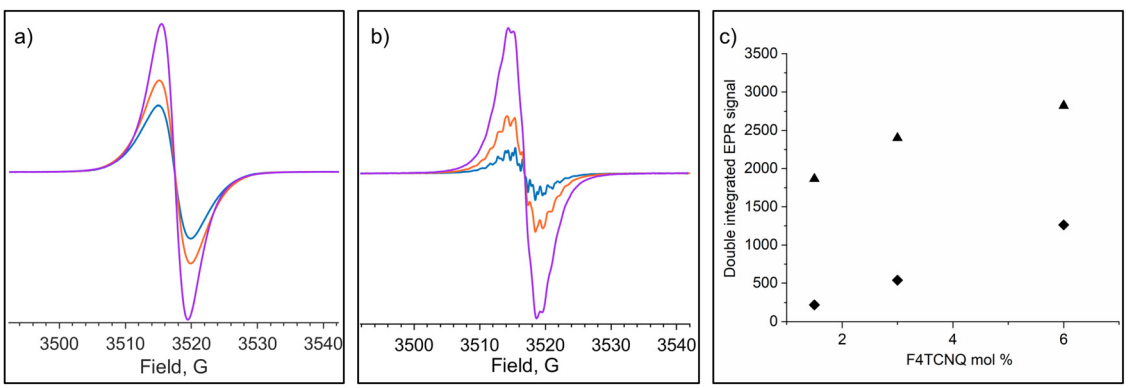

Fig. 2 EPR spectroscopy on spiro-OMeTAD solution, containing 1.5 mol% (blue), 3 mol% (orange) and 6 mol% (purple) of F4TCNQ as a dopant in acetonitrile prepared with (a) spiro-OMeTAD in chloroform and (b) spiro-OMeTAD in chlorobenzene. (c) Dependence of spiro-OMeTAD$^{\bullet+}$ formation obtained by double integrating EPR derivative signal on doping concentration of F4TCNQ in chlorobenzene (diamonds) and chloroform (triangles).

EPR spectroscopy of spiro-OMeTAD thin films on glass substrate

Spiro-OMeTAD films peak assignment. The use of spiro-OMeTAD as an HTM material in the perovskite cell necessitates its use in the form of a film. In determining the capacity of F4TCNQ as a dopant in spiro-OMeTAD films with EPR spectroscopy, spiro-OMeTAD thin films with 1.5 mol% F4TCNQ on glass were prepared. In order to provide a comparison with other common dopants used in perovskite solar cells, thin films of spiro-OMeTAD in chlorobenzene, containing LiTFSI, *t*BP, FK209 were also investigated.

All the spiro-OMeTAD films were prepared as described in the method section and presented in Fig. 3 with spiro-OMeTAD films containing LiTFSI, *t*BP and FK209 (spectrum a) and F4TCNQ (spectrum b). The spectra show a central derivative signal at *g* value of 2.0032 (3501 G), and a smaller signal (marked with an *) at a *g* value of 2.0101 (3490 G). The central signal at *g* value of 2.0032 is assigned to the radical cation of spiro-OMeTAD, spiro-OMeTAD$^{\bullet+}$ as it has been assigned in previous studies.[28–30] The two spectra look different with larger contribution from the central line in spiro-OMeTAD$^{\bullet+}$ with F4TCNQ.

EPR spectrum for spiro-OMeTAD containing F4TCNQ (Fig. 3, spectrum b) looks different from the solution EPR spectrum (Fig. 2a, blue spectrum) for the same solution concentration of the dopant (1.5 mol%). The smaller EPR signal (marked with an *) could be a residual contribution from the glass substrate (Fig. S1) or it could be a contribution from ^{14}N hyperfine couplings in spiro-OMeTAD as previously reported.[29] To understand this further, DFT calculations and simulations were performed.

Influence of increasing F4TCNQ dopant amount on spiro-OMeTAD films. The observations from the EPR measurements on spiro-OMeTAD solution with F4TCNQ show that F4TCNQ doping was more efficient for spiro-OMeTAD solution in chloroform. It is therefore necessary to evaluate the increase in the concentration of spiro-OMeTAD$^{\bullet+}$ in spiro-OMeTAD films prepared with varying dopant concentrations (0.5–6 mol%) of F4TCNQ in chloroform, compared to those prepared in chlorobenzene, and to further compare these results with films doped using the conventional additives LiTFSI, FK209 and *t*BP.

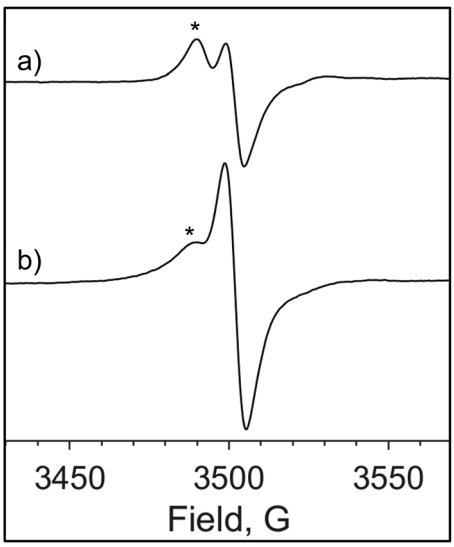

Fig. 3 EPR spectra of spiro-OMeTAD films deposited on glass prepared from spiro-OMeTAD solution in (a) chlorobenzene with dopants LiTFSI, *t*BP and FK209 and (b) chloroform with 1.5 mol% F4TCNQ.

EPR spectra from spiro-OMeTAD films with F4TCNQ, when spiro-OMeTAD is in chlorobenzene and chloroform and the corresponding concentration dependencies are presented in Fig. 4.

Spiro-OMeTAD films doped with F4TCNQ, prepared in chlorobenzene (Fig. 4a) and chloroform (Fig. 4b) are shown for molar ratio of 0.5 mol% (green), 1.5 mol% (blue), 3.0 mol% (orange) and 6.0 mol% (purple). All the EPR spectra in Fig. 4 show a central derivative signal at *g* value of 2.0032 (3501 G), additionally some of the spectra show a smaller signal at a *g* value of 2.0101 (3490 G). The central signal at *g* value of 2.0032 is assigned to the radical cation of spiro-OMeTAD, spiro-OMeTAD$^{\bullet+}$. The smaller signal at *g* value of 2.0101 could be a residual contribution remaining due to the glass substrate or it could be a contribution from ^{14}N hyperfine couplings in spiro-OMeTAD as mentioned before. In the case of spiro-OMeTAD films prepared in chloroform (Fig. 4b), the EPR spectrum at 0.5 mol% (green) looks similar to 1.5 mol% spiro-OMeTAD films prepared in chlorobenzene.

In the plot of concentration dependencies, for films prepared in chlorobenzene, the amount of spiro-OMeTAD$^{\bullet+}$ shows a continuous increase with increase in doping concentration of F4TCNQ (Fig. 4c). Spiro-OMeTAD films prepared in chloroform show an initial increase in the formation of spiro-OMeTAD$^{\bullet+}$ as the doping concentration of F4TCNQ increases, but at 6 mol% of F4TCNQ, there is already a levelling of the further increase. Amount of spiro-OMeTAD$^{\bullet+}$ in spiro-OMeTAD film prepared in chloroform is larger than the one prepared in chlorobenzene as confirmed from the double integrated EPR signal in Fig. 4c. This result corroborates the solution result (Fig. 2c) that doping capacity of F4TCNQ is better in chloroform. However, the difference in the amount of spiro-OMeTAD$^{\bullet+}$ is not constant through the two types of spiro-OMeTAD films (chloroform and chlorobenzene) over the doping concentrations of F4TCNQ. This indicates that the process of preparing spiro-OMeTAD films and therefore film properties influence the amount of spiro-OMeTAD$^{\bullet+}$ formation in the final film and both the dopant and substrate are influencing its formation. To understand the material properties of the spiro-OMeTAD films, UV/VIS spectroscopy and ellipsometry experiments were performed (see further below).

Influence of ambient air on spiro-OMeTAD films. The dopant F4TCNQ has been reported to be more stable against humidity as compared to the conventional dopants like LiTFSI, more commonly used in the perovskite solar cells.[15,16] To study the influence of humidity and oxygen on spiro-OMeTAD films, spiro-OMeTAD films prepared with F4TCNQ were exposed to ambient air for a week and EPR spectroscopy was measured at different time intervals during the week. This was compared

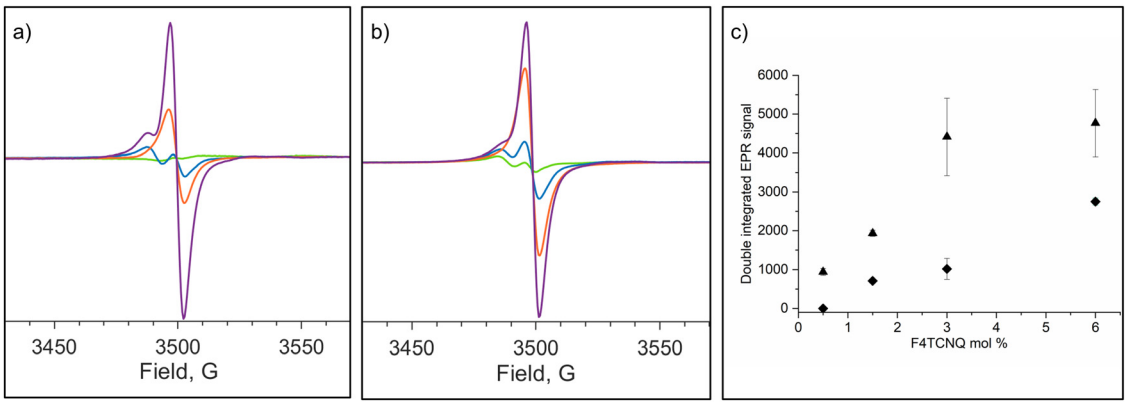

Fig. 4 EPR spectra of spiro-OMeTAD film on glass prepared from (a) spiro-OMeTAD solution in chlorobenzene and F4TCNQ in acetonitrile and (b) spiro-OMeTAD solution in chloroform and F4TCNQ in acetonitrile at 0.5 mol% (blue), 1.5 mol% (green), 3 mol% (orange) and 6 mol% (purple). (c) Dependence of spiro-OMeTAD$^{\bullet+}$ formation obtained by double integrating EPR derivative signal on doping concentration of F4TCNQ in chlorobenzene (diamonds) and chloroform (triangles).

with spiro-OMeTAD films in chlorobenzene containing LiTFSI, *t*BP and FK209.

In Fig. 5, EPR spectra on spiro-OMeTAD films with dopants LiTFSI, *t*BP and FK209 (Fig. 5a) and dopant F4TCNQ (Fig. 5b) after exposure to ambient air are presented. As has been described previously, both type of spiro-OMeTAD films show a central derivative signal at *g* value of 2.0032 (3501 G), and a smaller signal at a *g* value of 2.0101 (3490 G). The central signal at *g* value of 2.0032 is due to spiro-OMeTAD$^{\bullet+}$ present in the spiro-OMeTAD film. In spiro-OMeTAD films with dopants LiTFSI, *t*BP and FK209, the intensity of the central signal (Fig. 5a, day 0, spectrum in red) builds up as the week progresses and is maximum on day 7 (Fig. 5a, spectrum in green). On the other hand, in spiro-OMeTAD films containing dopant F4TCNQ (Fig. 5b), the intensity of the central signal is maximum on day 5 (Fig. 5b, day 0, spectrum in red).

In Fig. 5c, EPR signal area and hence the amount of spiro-OMeTAD$^{\bullet+}$ for two sets of samples is plotted *vs.* measurement on different days during the week. The amount of spiro-OMeTAD$^{\bullet+}$ changes differently for the two sets of dopants. In the spiro-OMeTAD film containing LiTFSI, *t*BP and FK209 (Fig. 5c, red circles), the amount of spiro-OMeTAD$^{\bullet+}$ shows an increase after the 5th day. In the case of spiro-OMeTAD film containing F4TCNQ (Fig. 5c, black circles), there is an increase in the amount of spiro-OMeTAD$^{\bullet+}$ on 5th day otherwise the same steady value is maintained. Thus, the influence of ambient air is different on the two different sets of dopants.

Also, considering the first day of the measurements, the amount of spiro-OMeTAD$^{\bullet+}$ is higher for spiro-OMeTAD film containing 1.5 mol% F4TCNQ than the film containing LiTFSI, *t*BP, FK209 (Fig. 5c). This effect is due to the use of chloroform as a solvent for preparing the spiro-OMeTAD films.

UV/VIS spectroscopy and ellipsometry of F4TCNQ-doped spiro-OMeTAD films. UV/VIS spectroscopy measurements using integrated sphere were performed on spiro-OMeTAD films prepared in chloroform containing varying (0–6 mol%) concentrations of the F4TCNQ dopant. The plot of absorptance (A) calculated by $A = (100 - T - R)\%$ for all the films and plotted against wavelength is shown in Fig. 6. The results show the characteristic peaks due to oxidized spiro-OMeTAD at 521 nm,

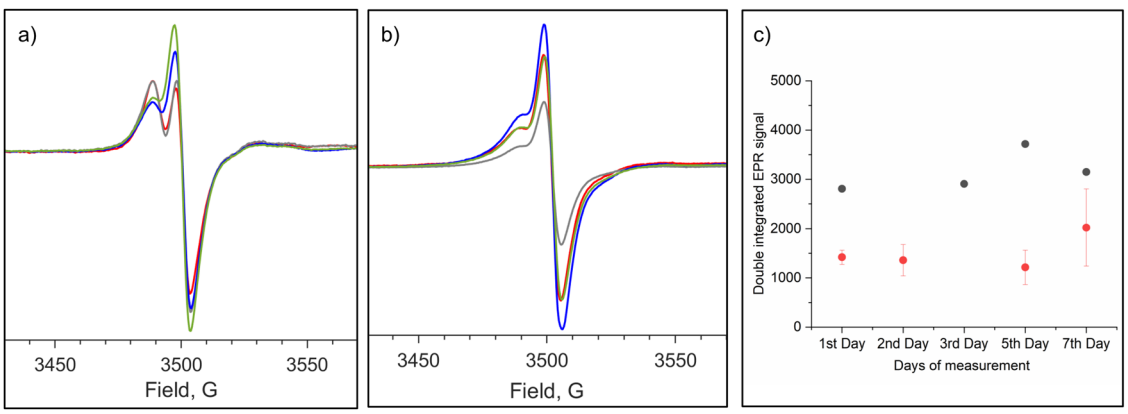

Fig. 5 EPR spectra of spiro-OMeTAD film on day 0 (red), day 2 (grey), day 5 (blue) and day 7 (green) prepared from spiro-OMeTAD solution (a) in chlorobenzene, containing LiTFSI, *t*BP and FK209 and (b) in chloroform, containing 1.5 mol% F4TCNQ. (c) Time dependence of spiro-OMeTAD$^{\bullet+}$ stability obtained by double integration of EPR derivative signal for spiro-OMeTAD films containing LiTFSI, *t*BP and FK209 (red circles) and F4TCNQ (black circles).

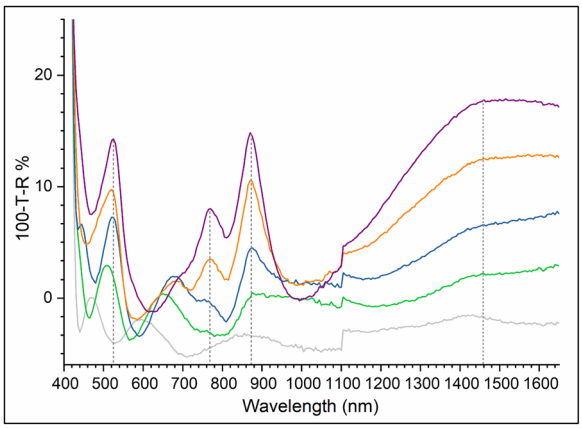

Fig. 6 UV/VIS spectroscopy on Spiro-OMeTAD films on glass prepared from solution in chloroform and F4TCNQ in acetonitrile at 0.5 mol% (green), 1.5 mol% (blue), 3 mol% (orange) and 6 mol% (purple) and no dopant (grey). The dotted lines are a guide for absorptance peak wavelength.

700 nm and 1500 nm[11,17–20,24,27] and a number of additional peaks. The peaks at 760 nm and 860 nm likely originate from the spiro-OMeTAD-F4TCNQ CT complex or the negative polaron of $F4TCNQ^{\bullet-}$.[14–16] The intensities of the two peaks increase with an increase in the dopant concentration (spectrum green to purple); thereby, confirming their correlation with the number of F4TCNQ molecules. The features observed in spiro-OMeTAD film with no dopant (grey) are possibly related to the interference effects.

The spiro-OMeTAD films were additionally characterized with SE measurements. To understand the variation in the EPR data, SE measurements were performed to determine the film thickness for F4TCNQ doped spiro-OMeTAD films.

To analyze the samples by SE, new samples of spiro-OMeTAD films were prepared in chloroform, containing varying (0–6 mol%) concentrations of the F4TCNQ dopant. The SE plus transmittance data was measured and individually modelled for each of the five samples. The film thicknesses obtained from these models are provided in Table 1.

An average thickness of 520 ± 50 nm is determined by SE measurements for spiro-OMeTAD films. Since the large variation is caused by the sample preparation, it is inherent in all the spiro-OMeTAD films. This would explain the variation in EPR signal observed for F4TCNQ doped spiro-OMeTAD films.

DFT calculations allow resolution of the EPR signal in the spiro-OMeTAD films. To determine the origin of the small EPR signal (marked with an *, Fig. 3) in spiro-OMeTAD films, DFT calculations were performed on spiro-OMeTAD molecule extracted from spiro-OMeTAD crystal structure.[32] EPR parameters were computed both before and after geometry optimization. The resulting g value and nitrogen hyperfine coupling constants were then used to simulate the EPR spectra of the spiro-OMeTAD films. The set of calculated EPR parameters that provided the best fit to the experimental spectra were obtained from the geometry optimized spiro-OMeTAD molecule and are summarized in Table 2. The corresponding spin density distribution (Fig. 7a) shows that the unpaired electron is asymmetrically localized on one arm of the molecule, primarily over two nitrogen atoms, consistent with previous reports.[25,29] The molecular Cartesian reference frame axes (red, blue and green) are shown in Fig. 7a with A-tensor principal-axis systems defined relative to the frame; their orientations specified by Euler angles in Table 2.

The EPR spectrum of spiro-OMeTAD in solution for chloroform could be simulated using isotropic g value and line width parameters. The line shape corresponds to a mixture of Gaussian and Lorentzian components. EPR spectra of spiro-OMeTAD in solution for chlorobenzene (Fig. S3) could be simulated considering contribution from $spiro\text{-}OMeTAD^{\bullet+}$ and $F4TCNQ^{\bullet-}$ and line shape a mixture of Gaussian and Lorentzian components.

EPR spectra from spiro-OMeTAD films containing dopants requires the contribution of the nitrogen hyperfine coupling constants to fit the broadening of the EPR spectrum in case of 3 mol% F4TCNQ (Fig. 7b) and the smaller EPR signal in case of 6 mol% F4TCNQ (Fig. 7c). However, in the EPR spectra from spiro-OMeTAD films containing 0.5 mol% and 1.5 mol% of F4TCNQ, it is not possible to completely fit the experimental spectra even after including the contribution of nitrogen hyperfine coupling constants. This indicates that there is residual contribution from glass left over in EPR signal from 0.5 mol% and 1.5 mol% of F4TCNQ spiro-OMeTAD films.

Table 1 Thickness obtained from SE measurements on F4TCNQ doped spiro-OMeTAD films on glass. Mean squared error (MSE) is also presented

Sample	Description	MSE	Thickness (nm)
Spiro-OMeTAD, no dopant	Glass + film	4.505	475
Spiro-OMeTAD + 0.5 mol% F4TCNQ	Glass + film	4.926	500
Spiro-OMeTAD + 1.5 mol% F4TCNQ	Glass + film	4.943	504
Spiro-OMeTAD + 3.0 mol% F4TCNQ	Glass + film	4.251	571
Spiro-OMeTAD + 6 mol% F4TCNQ	Glass + film	4.239	472

Table 2 g value and hyperfine parameters obtained from DFT calculation on a geometry optimized spiro-OMeTAD molecule extracted from spiro-OMeTAD crystal structure[32]

A-tensor principal values (MHz)				A_{iso} (MHz)	Euler angles (Deg)		
N_1	20.60	−0.72	−0.80	6.362	67.5	35.1	−71.5
N_2	−0.02	−0.00	0.02	0.001	−12.4	27.0	9.4
N_3	31.80	−0.52	−0.48	10.266	78.5	30.6	−78.8
N_4	0.03	−0.01	−0.02	0.001	−16.6	7.3	12.6
g-tensor principal values				g_{iso}			
	2.00182	2.00249	2.0037	2.0029			

Discussion

The formation of free charge carriers (holes) in spiro-OMeTAD directly influences the efficiency of the perovskite solar cell. The estimation of the number of holes is central to determining the dopant amount that needs to be used to produce $spiro\text{-}OMeTAD^{\bullet+}$. Dopants can additionally modify the material properties of the spiro-OMeTAD film in terms of film

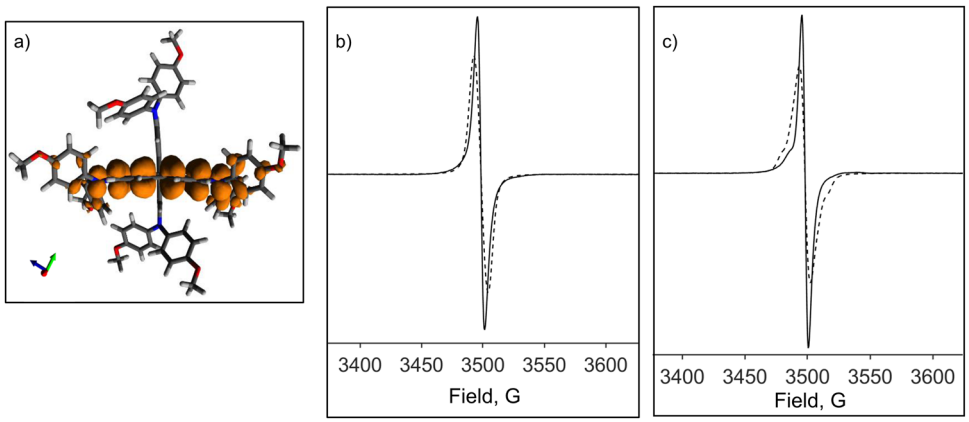

Fig. 7 (a) Electron Spin density distribution on a spiro-OMeTAD molecule obtained with DFT calculations after geometry optimization procedure. Comparison of the experimental (solid line) and simulated (dotted line) EPR spectra using the EASY SPIN package for spiro-OMeTAD films prepared in chloroform containing (b) 3.0 mol% F4TCNQ and (c) 6.0 mol% F4TCNQ. The axes (red, blue and green) shown in (a) refer to the molecular Cartesian reference frame. A-tensor principal-axis systems are defined relative to the frame; their orientations specified by Euler angles in Table 2.

morphology and interaction with the substrate. EPR spectroscopy performed on spiro-OMeTAD doped with F4TCNQ in solution and films provides important information on the influence of solvent on the doping of spiro-OMeTAD with F4TCNQ. The main findings of the study can be summarized as follows:

i. EPR spectroscopy is a robust method for characterizing doping in HTM films.

ii. The doping efficiency in spiro-OMeTAD films with F4TCNQ is dependent on the solvent used for film preparation.

iii. Influence of ambient air is observed on spiro-OMeTAD films in terms of stability.

iv. F4TCNQ is an effective p-type dopant for spiro-OMeTAD.

Below we discuss all these points and consider conditions for efficient doping of spiro-OMeTAD.

EPR spectroscopy as a robust method for characterizing doping in HTM films

EPR spectroscopy has been used to estimate the amount of spiro-OMeTAD$^{\bullet+}$ in spiro-OMeTAD films when F4TCNQ is used as the dopant. The measurements on spiro-OMeTAD films with *t*BP, LiTFSI and FK209 dopants were used to compare the efficiency of F4TCNQ. UV/VIS spectroscopy is the most commonly used method to characterize the spiro-OMeTAD films and to determine the doping efficiency of spiro-OMeTAD in solution and films. We would like to note that doping efficiency defined in this context is the amount of spiro-OMeTAD$^{\bullet+}$ holes present or produced chemically for a specified dopant concentration. This can be distinguished from the effective doping efficiency which is the amount of electrically mobile spiro-OMeTAD$^{\bullet+}$ holes and is only a part of the dopant concentration produced chemically.

EPR is a more robust and sensitive technique to estimate the amount of cation and anion radicals. Utilizing only UV/VIS spectroscopy to estimate spiro-OMeTAD$^{\bullet+}$ and F4TCNQ$^{\bullet-}$ would lead to more complicated data analysis. In case of UV/VIS spectroscopy spiro-OMeTAD$^{\bullet+}$ has two absorption bands at 520 and 1000 nm and F4TCNQ$^{\bullet-}$ has an absorption profile from 580 nm to 1000 nm.[14–16] So, with F4TCNQ$^{\bullet-}$ absorption overlapping with one of the absorption bands of spiro-OMeTAD$^{\bullet+}$, it becomes difficult to accurately estimate the amount of spiro-OMeTAD$^{\bullet+}$ and F4TCNQ$^{\bullet-}$. On the other hand, in EPR spectroscopy, both the radicals have very distinct profiles, so it is possible to separate them and estimate them in the same sample (solution or film).

Additionally, UV/VIS spectroscopy needs additional special conditions to be fulfilled for accurate determination of the amount of spiro-OMeTAD$^{\bullet+}$. It is necessary to know the molar absorptivity (ε) of each species in solid state and thickness of the thin films. Interference effects from the surface of the film can also distort the spectra. It is therefore, not completely straightforward to determine the amount of spiro-OMeTAD$^{\bullet+}$ with UV/VIS spectroscopy in thin films. EPR measurements are relatively easy to set up, and quantifying radical species does not require highly complex analysis. However, a few important considerations have to be made when using EPR spectroscopy (i) EPR detects electron spin states, making it unsuitable for estimating neutral species. Therefore, neutral charge-transfer complexes are not easily quantified using this method. (ii) EPR spectroscopy is a bulk measurement, so it is better for the substrate to have no background EPR signal. Also, EPR is an extremely sensitive technique for radical species, so sample variation and sample position change can produce a significant variation in the EPR spectra.

In the present study of the spiro-OMeTAD films with EPR spectroscopy, we observed a much larger variation in spiro-OMeTAD films prepared in chloroform (Fig. 4). This variation can be directly explained by film thickness variation. Ellipsometry has been used to determine thin film thickness for F4TCNQ doped spiro-OMeTAD films and an average thickness of 520 $\pm$ 50 nm was obtained for the films.

Doping efficiency of F4TCNQ in spiro-OMeTAD films is solvent dependent

EPR measurements on the dopant F4TCNQ in spiro-OMeTAD in the two solvents chlorobenzene and chloroform show a

marked difference in the amount of spiro-OMeTAD$^{\bullet+}$ that is formed. In the present study, a series of solvents were tried for a dissolution assessment and it was found that F4TCNQ was completely soluble in dichlorobenzene, chloroform and acetonitrile. Since spin coated spiro-OMeTAD films in perovskite solar cells are typically processed with LiTFSI and FK209 dopants introduced in acetonitrile, F4TCNQ was likewise dissolved in acetonitrile to ensure a consistent and directly comparable processing environment.

The EPR spectra on spiro-OMeTAD solution with F4TCNQ in chlorobenzene shows a distinctive peak due to F4TCNQ$^{\bullet-}$ at 1.5 and 3 mol% and as a splitting at 6 mol% of F4TCNQ in addition to spiro-OMeTAD$^{\bullet+}$ peak (Fig. 2b). The F4TCNQ$^{\bullet-}$ is observed as hyperfine splitting present in the spectrum for spiro-OMeTAD in chlorobenzene solution with its contribution simulated (Fig. S3). It is significant that in spiro-OMeTAD solution with F4TCNQ in chloroform however, no F4TCNQ$^{\bullet-}$ is observed. In EPR, the radicals, spiro-OMeTAD$^{\bullet+}$, F4TCNQ$^{\bullet-}$ or the CT complex of F4TCNQ-spiro-OMeTAD if it has a distinct ionic character can be observed.

The mechanism for formation of spiro-OMeTAD$^{\bullet+}$ by F4TCNQ has been suggested as:[15]

$$\text{Spiro-OMeTAD} - \text{F4TCNQ} \rightarrow \text{Spiro-OMeTAD}^{\bullet+} + \text{F4TCNQ}^{\bullet-} \quad (3)$$

In this mechanism, light is also considered for the dissociation of the spiro-OMeTAD- F4TCNQ CT complex. However, in our measurements, we did not observe any requirement for illumination in the formation of spiro-OMeTAD$^{\bullet+}$ by F4TCNQ. All samples were prepared and stored in dark vials to minimize exposure to ambient light. Therefore, based on our observations, light does not appear to be necessary for this process.

In the initial step of (3), F4TCNQ accepts an electron from spiro-OMeTAD to form the CT complex and then dissociates to give F4TCNQ$^{\bullet-}$ and spiro-OMeTAD$^{\bullet+}$.[14–16] For F4TCNQ to accept an electron, it has to be in the neutral form. F4TCNQ is present in the ionized form, F4TCNQ$^{\bullet-}$ in acetonitrile[36] (Fig. S2). Since acetonitrile is used to prepare the doped spiro-OMeTAD solutions, F4TCNQ$^{\bullet-}$ is likely present in the samples.

Considering the mechanism in (3), the EPR spectra of spiro-OMeTAD with dopant F4TCNQ in chlorobenzene could indicate two things. The observation of F4TCNQ$^{\bullet-}$ signifies that in chlorobenzene, not all F4TCNQ molecules form the CT complex with the spiro-OMeTAD molecules. The other option could be that F4TCNQ-spiro-OMeTAD complex dissociates immediately after being formed leading to F4TCNQ$^{\bullet-}$ being formed. Considering the first option, the amount of spiro-OMeTAD$^{\bullet+}$ formed would be less for the same amount of dopant in chlorobenzene as compared to other solvents. On the other hand, in the second option, even though the CT complex dissociates, there should be an upsurge in the formation of spiro-OMeTAD$^{\bullet+}$. We do not observe an upsurge but a decline in the formation of spiro-OMeTAD$^{\bullet+}$. This indicates that the F4TCNQ dopant does not work so efficiently in the chlorobenzene.

A comparison of the EPR spectra of spiro-OMeTAD in chloroform with 1.5 mol% of F4TCNQ dopant show no EPR signal contribution from F4TCNQ$^{\bullet-}$ as the same concentration of spiro-OMeTAD in chlorobenzene. Comparing the amount of spiro-OMeTAD$^{\bullet+}$ obtained from EPR signal area, the spiro-OMeTAD$^{\bullet+}$ in chloroform is 100 times more than the spiro-OMeTAD$^{\bullet+}$ formed in chlorobenzene. This indicates that the F4TCNQ dopant is very efficient in chloroform.

The evidence for this is additionally provided by a previous study which looked at stability of F4TCNQ in acetonitrile and chloroform.[36] It was observed in the study that F4TCNQ is present in the ionized form F4TCNQ$^{\bullet-}$ in acetonitrile and in the neutral form in chloroform. This would also explain the reason for the higher amount of spiro-OMeTAD$^{\bullet+}$ in chloroform. Chloroform stabilizes the neutral form of F4TCNQ and therefore even though F4TCNQ$^{\bullet-}$ can be formed in acetonitrile, once this solution is added to chloroform, more amount of electron transfer from spiro-OMeTAD to F4TCNQ takes place leading to a higher formation rate of spiro-OMeTAD$^{\bullet+}$ in chloroform. We however do not observe F4TCNQ$^{\bullet-}$ in chloroform, which may be attributed to aggregation effects. Another plausible explanation is the incomplete dissociation of the CT state. Under these conditions, F4TCNQ$^{\bullet-}$ remains localized in the vicinity of spiro-OMeTAD$^{\bullet+}$, while the positive charge resides on spiro-OMeTAD as a delocalized hole polaron. In both scenarios, solvent-induced effects render F4TCNQ$^{\bullet-}$ EPR silent, leading to the disappearance of its hyperfine structure. Solvent effects on the hyperfine couplings of free radicals in solution are well documented in the literature.[37–39] Accordingly, when spiro-OMeTAD$^{\bullet+}$ is considered as a delocalized hole polaron, the observed EPR signal is assigned to a F4TCNQ–Spiro-OMeTAD CT state with pronounced spiro-OMeTAD$^{\bullet+}$ polaron character.

Since, the higher amount of spiro-OMeTAD$^{\bullet+}$ is present in solution, which is used for spin coating and preparing the spiro-OMeTAD films, higher amount of spiro-OMeTAD$^{\bullet+}$ is determined in the spiro-OMeTAD films prepared from chloroform. Thus, the higher amount of spiro-OMeTAD$^{\bullet+}$ is maintained during the spin coating process indicating the presence of spiro-OMeTAD-F4TCNQ complex in the spiro-OMeTAD films. In UV/VIS spectroscopy on spiro-OMeTAD films, absorption peaks at 760 nm and 860 nm are observed. These peaks can be due to the presence of spiro-OMeTAD-F4TCNQ complex or F4TCNQ$^{\bullet-}$ polaron contribution. Since, in the EPR spectra obtained on the same spiro-OMeTAD films, we do not see any contribution from F4TCNQ$^{\bullet-}$ species, we assign these absorption peaks to the spiro-OMeTAD-F4TCNQ CT complex.

Influence of ambient air on F4TCNQ doped spiro-OMeTAD films

The spiro-OMeTAD films were exposed to ambient air and EPR spectra on these was measured. On exposure to ambient air, we are exposing the spiro-OMeTAD to humidity and oxygen. The mechanism of doping by F4TCNQ is different from LiTFSI. F4TCNQ can directly oxidize spiro-OMeTAD. In the case of LiTFSI, the oxidation of spiro-OMeTAD to spiro-OMeTAD$^{\bullet+}$,

occurs indirectly and requires the exposure of spiro-OMeTAD film to both light and oxygen. The influence of oxygen on F4TCNQ is therefore expected to be minimal. It is then relevant to know whether the oxidation process will continue once the films are kept in ambient air. The time period of the measurements was limited to a week. During this week, spiro-OMeTAD films doped with F4TCNQ showed almost a steady value with an increase on the 5th day. On the other hand, spiro-OMeTAD films doped with LiTFSI, *t*BP and FK209, showed an increase on the final day of the measurement. This agrees with what has been reported in the literature that F4TCNQ is more stable than LiTFSI[15,16] and for spiro-OMeTAD films doped with LiTFSI, *t*BP and FK209 show an increase during a week.[23,40] However, we only performed measurements over a one-week period, which limits our ability to assess the long-term stability of F4TCNQ compared to LiTFSI, *t*BP, and FK209 in terms of solar cell applications.

Since, F4TCNQ is a direct oxidizing agent for spiro-OMeTAD, increasing the amount of F4TCNQ, consequently oxidizes more amount of spiro-OMeTAD. This is different for the two solvents chloroform and chlorobenzene. The EPR spectra of spiro-OMeTAD in solution (Fig. 2c) in the case of chlorobenzene shows a linear increase in the amount of spiro-OMeTAD$^{\bullet+}$ with increasing mol% of F4TCNQ. However, in chloroform, this is not the case. Previous study has suggested a non-linear increase in the amount of spiro-OMeTAD$^{\bullet+}$ for mol% greater than 1% of F4TCNQ in chlorobenzene.[15] We however did not observe this. A point to note is that the EPR spectra of spiro-OMeTAD films prepared in chlorobenzene (Fig. 4c) do not exhibit this linear increase in spiro-OMeTAD$^{\bullet+}$. This difference could be caused due to material properties of the films as seen in the variation of thickness by the ellipsometry analysis.

F4TCNQ as a p-type dopant for spiro-OMeTAD

According to the EPR spectra on spiro-OMeTAD films, the spiro-OMeTAD$^{\bullet+}$ formed with F4TCNQ doping in chloroform was more than LITFSI, FK209 and *t*BP combined. The amount of spiro-OMeTAD$^{\bullet+}$ formed after 1.5 mol% F4TCNQ was used as a dopant is 2.5 times higher as compared to LiTFSI, FK209 and *t*BP combined. This is considering chloroform as the solvent. However, considering chlorobenzene, which has been used for LiTFSI, FK209 and *t*BP, then these dopants (LiTFSI, FK209, *t*BP) performed better than 1.5 mol% of F4TCNQ.

For 1.5 mol% of F4TCNQ, the amount of spiro-OMeTAD$^{\bullet+}$ formed in chloroform is 8 times more than chlorobenzene. At higher mol% of F4TCNQ, this increase reduces as a saturation sets in. In spiro-OMeTAD films, this can be clearly seen with maximum amount of spiro-OMeTAD$^{\bullet+}$ produced with 3 mol% of F4TCNQ. The amount of spiro-OMeTAD$^{\bullet+}$ from EPR spectra in solution also shows a linear increase till 3 mol% and then stabilization. It would be then beneficial to use spiro-OMeTAD in chloroform to get an optimum level of increase in the p-type doping of spiro-OMeTAD with a lower mol%, the best amount of F4TCNQ is in the range of 1.5 mol% to 3 mol%. On the other hand, to obtain a better efficiency of F4TCNQ with spiro-OMeTAD in chlorobenzene, it would be better to go to higher mol% concentration, preferably in the range of 2–6 mol%. The main advantage of using F4TCNQ is that it is a single dopant as compared to LiTFSI, FK209 and *t*BP which are three additives.

Conclusion

EPR spectroscopy is a powerful analytical tool for probing dopants in HTM solutions and thin films. The solvent-dependent behavior of F4TCNQ in chloroform significantly influences its doping efficiency in spiro-OMeTAD. Thus, understanding and characterizing the solvent interactions of dopants used in HTM thin films would lead to optimizing their performance in future perovskite and organic solar cell applications. F4TCNQ is proven to be an effective single component dopant for spiro-OMeTAD, offering valuable insights for further optimization of doped HTM layers.

Conflicts of interest

There are no conflicts of interest to declare.

Data availability

The data supporting the findings of this study are available within the article and its Supplementary Information (SI). Additional raw experimental and computational data are available from the corresponding author upon reasonable request.

Supplementary information (SI) is available. See DOI: https://doi.org/10.1039/d5cp04633e.

Acknowledgements

This work was supported by the Olle Engkvist Foundation (grant 222-056). Dr Byeong Jo Kim is thanked for his help and support. DFT calculations were performed using resources by the National Academic Infrastructure for Super-computing in Sweden (NAISS) (allocation no. NAISS 2025/5-94 and NAISS 2025/23-205) at the National Supercomputing Center in Linköping, Sweden.

References

1 J. H. Heo, S. H. Im, J. H. Noh, T. N. Mandal, C.-S. Lim, J. A. Chang, Y. H. Lee, H.-J. Kim, A. Sarkar and M. K. Nazeeruddin, *Nat. Photon.*, 2013, **7**, 486–491.
2 N. Pellet, P. Gao, G. Gregori, T. Y. Yang, M. K. Nazeeruddin, J. Maier and M. Grätzel, *Angew. Chem., Int. Ed.*, 2014, **53**, 3151–3157.
3 J. Y. Kim, J. W. Lee, H. S. Jung, H. Shin and N. G. Park, *Chem. Rev.*, 2020, **120**, 7867–7918.
4 A. K. Jena, A. Kulkarni and T. Miyasaka, *Chem. Rev.*, 2019, **119**, 3036–3103.
5 M. M. Lee, J. Teuscher, T. Miyasaka, T. N. Murakami and H. J. Snaith, *Science*, 2012, **338**, 643–647.

6 J. Y. Han, K. Park, S. Tan, Y. Vaynzof, J. J. Xue, E. W. G. Diau, M. G. Bawendi, J. W. Lee and I. Jeon, *Nat. Rev. Methods Primers*, 2025, **5**, 3.
7 Y. Y. Dong, F. M. Rombach, G. H. Min, H. J. Snaith, C. T. Lin, S. A. Haque and T. J. Macdonald, *Mater. Sci. Eng., R*, 2025, **162**, 100875.
8 Z. Hawash, L. K. Ono and Y. Qi, *Adv. Mater. Interfaces*, 2018, **5**, 1700623.
9 L. Nakka, Y. Cheng, A. G. Aberle and F. Lin, *Adv. Energy Sustainable Res.*, 2022, **3**, 2200045.
10 N. A. N. Ouedraogo, G. O. Odunmbaku, B. Guo, S. S. Chen, X. X. Lin, T. Shumilova and K. Sun, *ACS Appl. Mater. Interfaces*, 2022, **14**, 34303–34327.
11 U. B. Cappel, T. Daeneke and U. Bach, *Nano Lett.*, 2012, **12**, 4925–4931.
12 C. C. Boyd, R. Cheacharoen, T. Leijtens and M. D. McGehee, *Chem. Rev.*, 2019, **119**, 3418–3451.
13 J. Krüger, R. Plass, L. Cevey, M. Piccirelli, M. Grätzel and U. Bach, *Appl. Phys. Lett.*, 2001, **79**, 2085–2087.
14 D. Y. Chen, W. H. Tseng, S. P. Liang, C. I. Wu, C. W. Hsu, Y. Chi, W. Y. Hung and P. T. Chou, *Phys. Chem. Chem. Phys.*, 2012, **14**, 11689–11694.
15 L. Huang, Z. Hu, J. Xu, K. Zhang, J. Zhang, J. Zhang and Y. Zhu, *Electrochim. Acta*, 2016, **196**, 328–336.
16 J. S. Luo, C. Y. Jia, Z. Q. Wan, F. Han, B. W. Zhao and R. L. Wang, *J. Power Sources*, 2017, **342**, 886–895.
17 W. H. Nguyen, C. D. Bailie, E. L. Unger and M. D. McGehee, *J. Am. Chem. Soc.*, 2014, **136**, 10996–11001.
18 S. Wang, W. Yuan and Y. S. Meng, *ACS Appl. Mater. Interfaces*, 2015, **7**, 24791–24798.
19 R. L. Forward, K. Y. Chen, D. M. Weekes, D. J. Dvorak, Y. Cao and C. P. Berlinguette, *ACS Energy Lett.*, 2019, **4**, 2547–2551.
20 M. J. Grotevent, Y. Lu, T. Šverko, M.-C. Shih, S. Tan, H. Zhu, T. Dang, J. K. Mwaura, R. Swartwout, F. Beiglböck, L. Kothe, V. Bulović and M. G. Bawendi, *Adv. Energy Mater.*, 2024, **14**, 2400456.
21 R. Schölin, M. H. Karlsson, S. K. Eriksson, H. Siegbahn, E. M. J. Johansson and H. Rensmo, *J. Phys. Chem. C*, 2012, **116**, 26300–26305.
22 E. J. Juarez-Perez, M. R. Leyden, S. H. Wang, L. K. Ono, Z. Hawash and Y. B. Qi, *Chem. Mater.*, 2016, **28**, 5702–5709.
23 A. Abate, T. Leijtens, S. Pathak, J. Teuscher, R. Avolio, M. E. Errico, J. Kirkpatrik, J. M. Ball, P. Docampo, I. McPherson and H. J. Snaith, *Phys. Chem. Chem. Phys.*, 2013, **15**, 2572–2579.
24 U. B. Cappel, E. A. Gibson, A. Hagfeldt and G. Boschloo, *J. Phys. Chem. C*, 2009, **113**, 6275–6281.
25 D. Shi, X. Qin, Y. Li, Y. He, C. Zhong, J. Pan, H. L. Dong, W. Xu, T. Li, W. P. Hu, J. L. Brédas and O. M. Bakr, *Sci. Adv.*, 2016, **2**, e1501491.
26 W. Zhang, L. Q. Wang, Y. Guo, B. B. Zhang, V. Leandri, B. Xu, Z. F. Li, J. M. Gardner, L. C. Sun and L. Kloo, *Chem. Commun.*, 2020, **56**, 1589–1592.
27 G. Szabó and P. V. Kamat, *ACS Energy Lett.*, 2024, **10**, 330–336.
28 M. Namatame, M. Yabusaki, T. Watanabe, Y. Ogomi, S. Hayase and K. Marumoto, *Appl. Phys. Lett.*, 2017, **110**, 123904.
29 U. M. H. Yasin, *Paramagnetic States in Organic and Perovskite Solar Cells: From Chemical Doping to Spin-Dependent Transport*, Freie Universitaet Berlin, Germany, 2019.
30 F. Lamberti, T. Gatti, E. Cescon, R. Sorrentino, A. Rizzo, E. Menna, G. Meneghesso, M. Meneghetti, A. Petrozza and L. Franco, *Chem*, 2019, **5**, 1806–1817.
31 S. Stoll and A. Schweiger, *J. Magn. Reson.*, 2006, **178**, 42–55.
32 Y. Li, H. Y. Li, C. Zhong, G. Sini and J. L. Brédas, *npj Flex. Electron.*, 2017, **1**, 2.
33 F. Neese, *Wiley Interdiscip. Rev.: Comput. Mol. Sci.*, 2012, **2**, 73–78.
34 L. Misseeuw, A. Krajewska, I. Pasternak, T. Ciuk, W. Strupinski, G. Reekmans, P. Adriaensens, D. Geldof, F. Blockhuys, S. Van Vlierberghe, H. Thienpont, P. Dubruel and N. Vermeulen, *RSC Adv.*, 2016, **6**, 104491–104501.
35 M. Arvind, C. E. Tait, M. Guerrini, J. Krumland, A. M. Valencia, C. Cocchi, A. E. Mansour, N. Koch, S. Barlow, S. R. Marder, J. Behrends and D. Neher, *J. Phys. Chem. B*, 2020, **124**, 7694–7708.
36 A. Rubino, A. Camellini and I. Kriegel, *Opt. Mater. X*, 2021, **11**, 100081.
37 P. Ludwig, R. N. Adams and T. Layloff, *J. Am. Chem. Soc.*, 1964, **86**, 4568–4573.
38 E. G. Janzen, G. A. Coulter, U. M. Oehler and J. P. Bergsma, *Can. J. Chem.*, 1982, **60**, 2725–2733.
39 G. Audran, L. Bosco, P. Brémond, T. Butscher, J. M. Franconi, K. Kabitaev, S. R. A. Marque, P. Mellet, E. Parzy, M. Santelli, E. Thiaudière and S. Viel, *RSC Adv.*, 2016, **6**, 5653–5670.
40 Y. Cho, H. D. Kim, J. H. Zheng, J. M. Bing, Y. Li, M. Zhang, M. A. Green, A. Wakamiya, S. J. Huang, H. Ohkita and A. W. Y. Ho-Baillie, *ACS Energy Lett.*, 2021, **6**, 925–933.